# The Late Quaternary Glaciations as the Response of a Three-Component Feedback System to Earth-Orbital Forcing

BARRY SALTZMAN, ANTHONY R. HANSEN[1] AND KIRK A. MAASCH

*Department of Geology and Geophysics, Yale University, New Haven, CT 06511*

(Manuscript received 21 February 1984, in final form 21 August 1984)

ABSTRACT

A climatic feedback system previously described, consisting of three prognostic nonlinear equations governing the mass of ice sheets $\zeta$, the mass of marine and continental marginal ice $\chi$, and the mean ocean temperature $\theta$ is forced by a representation of the effects of external earth-orbital variations. With reasonable amplitudes for the eccentricity, obliquity, and precession forcing, the free oscillatory solutions of major period near 100 kyr can be modified in a way that substantially agrees with the $\delta^{18}$O-derived observations of ice mass evolution. In particular, a proper structure, variance spectrum, and "phase lock" of the major variations are obtained over the last 400 kyr. An analysis of the sensitivity of these results to variations in the model parameters and to random perturbations shows that the solution is robust for small changes in all but a few of the equation coefficients. Concomitant variability in the marine ice mass, ocean temperature and net radiation at the top of the atmosphere are predicted, the signatures of which must be sought in the geological records to check the validity of the model. An independent estimate of the variations of ocean temperature $\theta$, derived with plausible assumptions from the difference between the solution for $\zeta$ and the $\delta^{18}$O record, is shown to be compatible with the solution obtained for $\theta$.

## 1. Introduction

It has been shown that a three-component dynamical system containing physically plausible feedbacks can be constructed to yield *free* oscillatory behavior qualitatively similar in many respects to the long-period Quaternary ice mass variations inferred from $\delta^{18}$O records (Saltzman and Sutera, 1984, henceforth called SS). There is strong evidence, however, that these $\delta^{18}$O records contain the signatures of earth-orbital periodic *forcing* that acts as a "pacemaker" of the main variations (Hays *et al.*, 1976; Imbrie *et al.*, 1984). It is our purpose here to explore the extent to which earth-orbital forcing of the SS feedback system can replicate the observed record.

## 2. The $\zeta$–$\chi$–$\theta$ system

The three components involved in the SS model are: $\zeta$, the deep continental ice-sheet mass; $\chi$, the mass of all forms of marine ice ranging from shelves to sea ice (that we can perhaps extend to include thinner, more active layers of continental ice particularly near the margins of the deep ice sheets); and $\theta$, the mean temperature of the world ocean the signature of which is perhaps to be found in the depth and temperature of the low-latitude mixed layer. A pictorialization of the system is shown in Fig. 1. This figure also includes two additional slow variables, $h$ (ice topography) and $\epsilon$ (bedrock depression), that we do not consider explicitly in this model but which are major variables in other dynamical models of ice age evolution that have been able to replicate the dominant near-100 kyr variations (e.g., Oerlemans, 1980, 1982; Birchfield *et al.*, 1981; Pollard, 1982, 1983a,b; LeTreut and Ghil, 1983; Peltier and Hyde, 1984).

The equations postulated to govern the departures from equilibrium (denoted by primes) of our $\zeta$–$\chi$–$\theta$ system are the same as given in SS; i.e.,

$$\frac{d\zeta'}{dt} = a_0\zeta' + a_1(1 - a_2\chi')\chi' - a_3\theta' + F_\zeta + R_\zeta, \quad (1)$$

$$\frac{d\chi'}{dt} = b_0\zeta' + b_1(1 - b_2\chi' - b_3\chi'^2 - b_4\zeta'^2)\chi' - b_5\theta' + F_\chi + R_\chi, \quad (2)$$

$$\frac{d\theta'}{dt} = c_0\zeta' + c_1\chi' - c_2\theta' + F_\theta + R_\theta, \quad (3)$$

where $F$ and $R$ denote additive periodic and stochastic forcing, respectively, and the coefficients $a$, $b$, and $c$ are positive constants. The physical processes assumed to be associated with each of these coefficients are discussed in SS.

The free solution, obtained with no periodic or stochastic forcing, is shown in Fig. 2 using the same values of the coefficients given in SS with the exception

[1] Present affiliation: Meteorology Research Center, Control Data Corporation, Minneapolis, MN 55440.

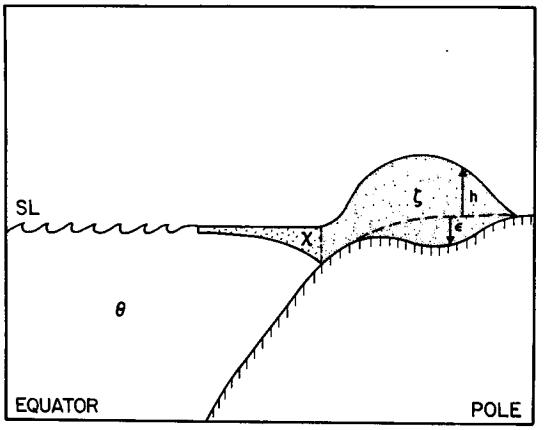


FIG. 1. Schematic meridional cross section of the climatic system showing the three prognostic variables governed by our model: $\zeta$ (ice sheet mass), $\chi$ (marine and continental "marginal" ice mass), and $\theta$ (mean ocean temperature). Other potentially important prognostic variables not treated explicitly in this model are isostatic bedrock depression $\epsilon$, and ice thickness $h$.

of $a_1$ and $c_2$; that is, $a_0 = 0$, $a_1 = 2.96 \times 10^{-4}\ ZX^{-1}$ yr$^{-1}$ (SS value was $2.90 \times 10^{-4}\ XZ^{-1}$ yr$^{-1}$), $a_2 = 1.86\ X^{-1}$, $a_3 = 7.59 \times 10^{-6}\ Z\Theta^{-1}$ yr$^{-1}$, $b_0 = 1.38 \times 10^{-4}\ XZ^{-1}$ yr$^{-1}$, $b_1 = 3.77 \times 10^{-4}$ yr$^{-1}$, $b_2 = 1.58 \times 10^{-1}\ X^{-1}$, $b_3 = 3.77\ X^{-2}$, $b_4 = 17.88\ Z^2$, $b_5 = 2.09 \times 10^{-4}\ X\Theta^{-1}$ yr$^{-1}$, $c_0 = 1.32 \times 10^{-4}\ \Theta Z^{-1}$ yr$^{-1}$, $c_1 = 9.55 \times 10^{-6}\ \Theta X^{-1}$ yr$^{-1}$, $c_2 = 1.45 \times 10^{-4}$ yr$^{-1}$ (SS values were 1.00 and $1.54 \times 10^{-4}$ yr$^{-1}$), where $Z$, $X$, and $\Theta$ are arbitrary ranges of $\zeta$, $\chi$, and $\theta$, respectively, as estimated from geological evidence. The new value of $c_2$ corresponds to a thermal response time $c_2^{-1}$ = 6900 yr rather than the 10 000 and 6500 yr values used in SS. Plausible magnitudes are $Z \approx 5 \times 10^{19}$ kg, $X \approx 10^{18}$ kg (increased from that suggested in SS because of the inclusion of 'marginal' continental ice along with purely marine forms), and $\Theta \approx 3$ K.

Although this free solution has some features that are in qualitative agreement with the inferred ice mass record (notably variations of around 100 ky period with rapid deglaciations), it certainly is more regular and cyclic than actually observed, is lacking in any response in the near-20 and 40 kyr periods as observed, and the periodic variations are of *arbitrary phase*. In the following sections we examine the degree to which orbital forcing can improve the solution in these regards.

## 3. Orbital forcing

The long-term variations in the magnitude and geographical distribution of incoming external solar radiation, due to variations in eccentricity, precession, and obliquity of the earth are known with a high degree of accuracy (Milankovitch, 1920; Vernekar, 1972; Berger, 1977). To translate these known variations into forcing functions for the internal variables $\zeta$, $\chi$ and $\theta$, however, requires a degree of understanding that we are far from possessing. In this regard we make the following general remarks and assumptions.

1) The eccentricity variations, with major periods near 100 and 400 kyr, are the only ones that lead to a *net* increase and decrease of total energy impinging on the earth, these changes having an amplitude of the order of $10^{-1}$ W m$^{-2}$. This is not insignificant compared to the net global latent heat release and consumption involved in long-term Quaternary ice variations which are at most also of the order of $10^{-1}$ W m$^{-2}$ (Saltzman, 1983). However, the greater part of this forcing amplitude is made unavailable for water phase changes and heat storage by compensating changes in outgoing longwave radiation that lead to rapid equilibration of the atmosphere and upper layer of the earth and ocean. Thus, we can expect relatively little direct forcing of the deep cryosphere and oceans by these variations. We shall assume here that radiative equilibrium prevails to within only one percent of the eccentricity-induced global solar radiation variations (e.g., $10^{-3}$ W m$^{-2}$) and only this amount can be utilized for ice production and melting. Moreover, we assume this small amount is utilized only by ice in its most sensitive form, namely marine/marginal ice measured by $\chi$. We also assume that there is no

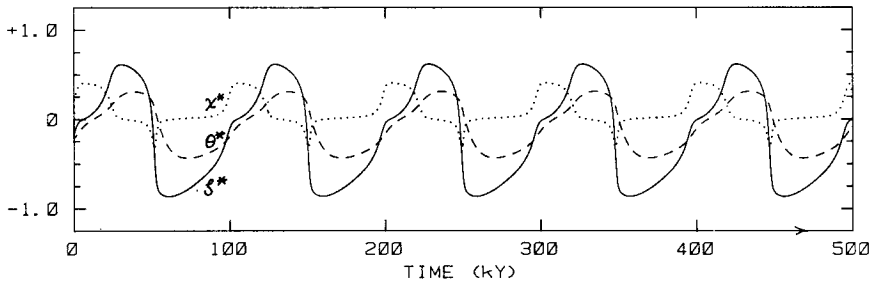


FIG. 2. *Free* solution of the $\zeta$–$\chi$–$\theta$ system, (1), (2) and (3), for the coefficient values given in Section 2, in terms of the nondimensional values $\zeta^* = 1.45\ Z^{-1}\ \zeta'$, $\chi^* = 0.75\ X^{-1}\ \chi'$, and $\theta^* = 0.96\ \Theta^{-1}\ \theta'$ where $Z$, $X$, and $\Theta$ are arbitrary characteristic ranges of $\zeta'$, $\chi'$, and $\theta'$ during the Quaternary.

significant forcing of the mean ocean temperature $\theta$ by these variations, this being a departure from the assumption made in Saltzman *et al.* (1984).

2) Although the precessional and obliquity variations do not lead to a *net* energy flux into or out of the complete climatic system, they do lead to relatively high amplitude (i.e., O[10 W $m^{-2}$] variations in the geographical distribution of incoming solar radiation (e.g., Kutzbach, 1981). It is not unreasonable to expect that the general circulation of the atmosphere and oceans can be affected in a way that leads to enhanced melting or freezing of ice, again mainly in the form of the more sensitive 'marginal/marine' ice mass measured by $\chi$, and that these effects can be an order of magnitude greater than the eccentricity effects (e.g., $10^{-2}$ W $m^{-2}$).

Thus we shall assume here (i) that the orbital forcing operates on the complete dynamical system through a primary effect on the $\chi$-component, that is,

$$F_\zeta = F_\theta = 0, \tag{4}$$

and, (ii) that

$$F_\chi = -[\alpha A(t) + \beta B(t) + \gamma C(t)], \tag{5}$$

where $A(t)$, $B(t)$ and $C(t)$ are, respectively, the normalized eccentricity ($e$), obliquity ($\epsilon$), and precession index ($-\Delta e \sin\omega$) variations with time computed by Berger (1977), discussed and pictured by Imbrie *et al.* (1984) and reproduced here in Fig. 3. The amplitudes $\alpha$, $\beta$ and $\gamma$ assigned to these functions are to be tuned, in accordance with the above remarks, to give a good fit of the solution to the observations consistent with the following order of magnitude estimates:

$$\alpha = \mathrm{O}[10^{-3}\ \mathrm{W\ m^{-2}} \times \sigma L_f^{-1}] = \mathrm{O}[10^{13}\ \mathrm{kg\ yr^{-1}}], \tag{6}$$

$$\beta, \gamma = \mathrm{O}[10^{-2}\ \mathrm{W\ m^{-2}} \times \sigma L_f^{-1}] = \mathrm{O}[10^{14}\ \mathrm{kg\ yr^{-1}}], \tag{7}$$

where $\sigma$ is the area of the earth ($5 \times 10^{14}$ $m^2$) and $L_f$ is the latent heat of fusion ($3.34 \times 10^5$ J $kg^{-1}$).

## 4. Results

In Fig. 4 we show the solution for $\zeta'$ in nondimensional units, $\zeta^* = 1.45\ Z^{-1}\ \zeta'$, obtained for the system (1), (2), and (3) when forcing of the form (5) is applied, keeping all coefficients the same as were used to deduce the free solution shown in Fig. 3. The values of the forcing amplitudes used are:

$$\left.\begin{aligned} \alpha &= \alpha_0 = 7 \times 10^{-6}\ X\ \mathrm{yr^{-1}} \\ \beta &= \beta_0 = 59 \times 10^{-6}\ X\ \mathrm{yr^{-1}} \\ \gamma &= \gamma_0 = 134 \times 10^{-6}\ X\ \mathrm{yr^{-1}} \end{aligned}\right\},$$

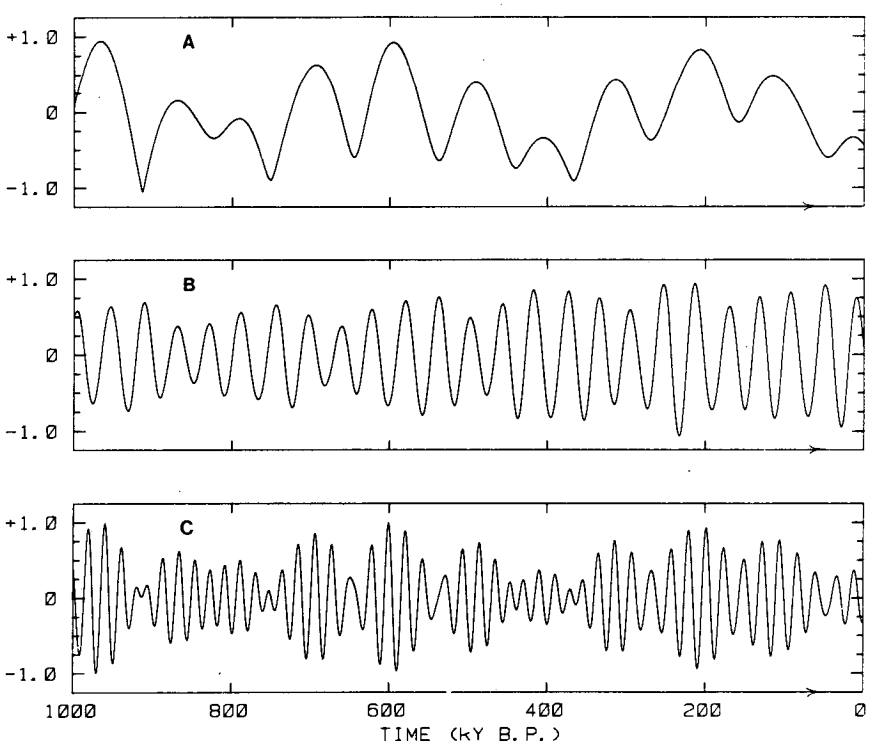


FIG. 3. Normalized variations in eccentricity (A), obliquity (B), and precession index (C), over the last 1 Myr, from Berger (1977). Positive values represent conditions believed to result in net warming or melting of ice in the Northern Hemisphere. (See Imbrie *et al.*, 1984, Fig. 2).

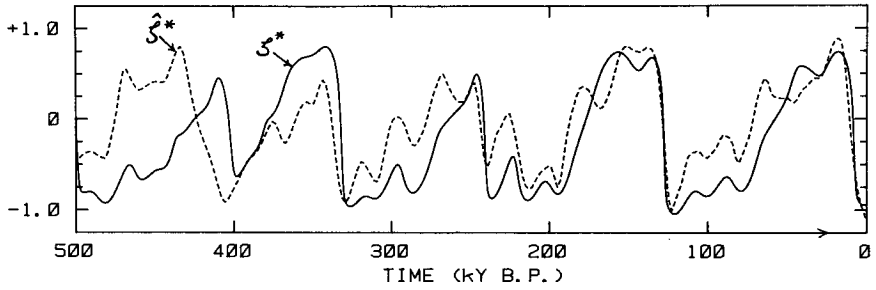


FIG. 4. Solid curve: Forced solution for $\zeta'$ of the system (1), (2), and (3) with amplitudes $\alpha_0$, $\beta_0$, $\gamma_0$ of $A(t)$, $B(t)$ and $C(t)$, respectively, given in Section 4. Nondimensional units shown are $\zeta^* = 1.45\ Z^{-1}\ \zeta'$. Dashed curve: SPECMAP reconstruction of ice mass variations over the last 500 kyr, $\hat{\zeta}^*$, derived from $\delta^{18}O$ observations (Imbrie *et al.*, 1984) assuming no effects of ocean temperature change and with tuning assumptions regarding the obliquity and precessional variations. The time coordinate is in units of kyr BP (before present), increasing to the right as in Fig. 2.

all of which are of the order of magnitude suggested as being reasonable in the previous section if $X \approx 10^{18}$ kg. With these values of $\alpha$, $\beta$ and $\gamma$ the complete forcing function $F_x$ is of the form shown as the solid curve in Fig. 5; for comparison, the solution for $\zeta'$ shown in Fig. 4 is repeated here (dashed curve). The particular values of $\alpha$, $\beta$ and $\gamma$ chosen were selected to give a relatively robust solution that can show qualitative agreement with the $\delta^{18}O$ chronology constructed by the SPECMAP group (Imbrie *et al.*, 1984) given also in nondimensional units by the dashed curve in Fig. 4. According to Imbrie *et al.*, this $\delta^{18}O$ curve is due primarily to changes in ice mass. In scaling this SPECMAP "ice curve" (which we call $\hat{\zeta}^*$) relative to our solution $\zeta^*$ we have assumed a rough agreement in amplitude between $\zeta^*$ and $\hat{\zeta}^*$ particularly over the last two relatively well-defined glacial cycles.

Since the "correct" values of $\alpha$, $\beta$ and $\gamma$ imply net global energy fluxes of less than $10^{-1}$ W m$^{-2}$ they cannot be determined from any deductive physical calculation; hence, we believe the above inductive procedure is the only reasonable means for arriving at the forcing amplitudes within the context of our model. Note that our particular weighting factors $\alpha_0$, $\beta_0$, and $\gamma_0$ are much different than the 1–1–1 weighting used by Imbrie *et al.* (1984) to construct their "ETP" forcing curve. There is, of course, the further question of "sensitivity" of the solution to small (e.g., ±10 percent) changes in these values; in our case such changes in any coefficient do not lead to any perceptable changes in the evolution. In Section 5 we discuss the more general sensitivity and robustness properties of our solution. At this point we note that the solution shows no structural changes for white noise forcing of amplitudes as high as $|R_x| = 8 \times 10^{-5}\ X\ \text{yr}^{-1}$. Moreover, to achieve the solutions shown in Fig. 4, the runs were started at 1 Myr with the forcing shown in Fig. 3, for *arbitrary, randomly-varied,* initial conditions. Although there were differences in the solution over the first few hundred kyr depending on the initial conditions, in all cases the solution "locked in" to the solution shown in Fig. 4 over the last 500 kyr BP (before present).

As we have noted the twelve nonzero coefficients in (1)–(3) determine only the structural form and period of the main free behavior of the 3-variable system, not the observed details of the ice mass variations inferred from the $\delta^{18}O$ record. Actually, it can be shown that only three or four independent nondimensional numbers representing combinations of these coefficients determine the eigenvalue vector

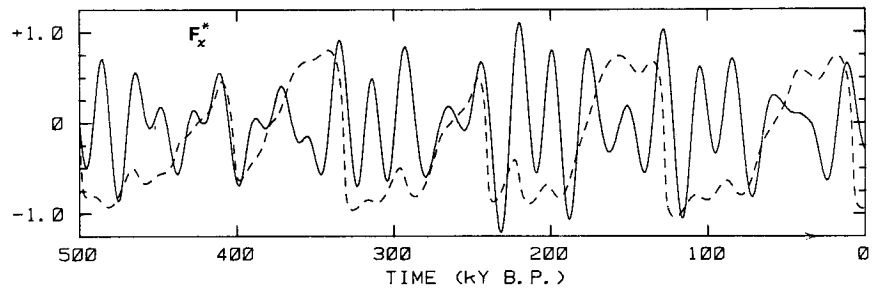


FIG. 5. Solid curve: The composite forcing function, in nondimensional units, $F_x^* = \{6 \times 10^3\ \text{yr}\ [X\ (\text{kg})]^{-1}\}\ F_x(t)$. Dashed curve: Forced solution for $\zeta'$, in nondimensional units $\zeta^* = 1.45\ Z^{-1}\ \zeta'$, as in Fig. 4.

at the "center manifold" needed to produce this structural form. The particular coefficients appearing in (1)–(3) have been apportioned to accomodate the conceptual physical processes believed to be operative from the qualitative geological evidence. In judging the "parsimony" of our representation it should be remembered that we are generating not only the continental ice sheet variations $\zeta$, with these coefficient choices, but also two additional physical variables, $\chi$ and $\theta$. In any event, the parameters to be specified here are certainly much fewer than would be needed in a time-dependent GCM or statistical dynamical model (e.g., Saltzman and Moritz, 1980). The details of the SPECMAP $\hat{\zeta}$*-curve are reproduced to the extent shown in Fig. 4 by three additional weighting coefficients $\alpha$, $\beta$, $\gamma$. However, the SPECMAP data (Imbrie *et al.*, 1984) are already tuned to contain the obliquity (41 kyr) and precessional (19 and 23 kyr) variations given by $B(t)$ and $C(t)$, so the inclusion of these two forcing terms in our model is at least partially required by the properties of the data itself. What is of significance here is the degree to which this same input forcing to our 3-component nonlinear internal system given by (1), (2) and (3), plus the weak eccentricity forcing, can simulate these frequencies in the SPECMAP reconstruction as well as all the other variations that are of even larger amplitude with a period near 100 kyr. We can view the amplification of the weak forcing near 100 kyr period as being the consequence of the robust free oscillatory behavior of the model climatic system near this period. Note that although the eccentricity forcing is extremely small ($10^{-3}$ W m$^{-2}$) the observed fluctuations in the storage of latent heat of fusion over the better part of the 100 kyr cycle are also extremely small ($10^{-2}$ W m$^{-2}$).

In Fig. 6 we show the variance spectra for the forcing function $F_\chi$ (top), the free $\zeta'$-solution (middle, solid curve), the forced $\zeta'$-solution (bottom, solid curve), and the SPECMAP reconstruction of $\zeta$ (middle and bottom, dashed curves). The spectrum of the forcing function is based on the 1 Myr time series shown in Fig. 5, while the spectra of $\zeta$ are all based on the 500 kyr time series. It would appear that the general character of the spectrum of the ice mass evolution over this period is fairly well replicated by the forced solution. From Fig. 5 we see that, as noted by Broecker (1984), the last four major deglaciations all occur during periods when $F_\chi$ is large (i.e., when there is a tendency for warm Northern Hemisphere summers due to precession and obliquity changes and high net incoming radiation due to eccentricity changes); this undoubtedly accounts in large measure for the "pacemaking" or, more properly, "phase-locking" role of the external forcing. It can also be seen from Fig. 5 that there is a roughly 90° phase lag between the forcing and ice mass response at the high-amplitude precessional period of about 20 kyr.

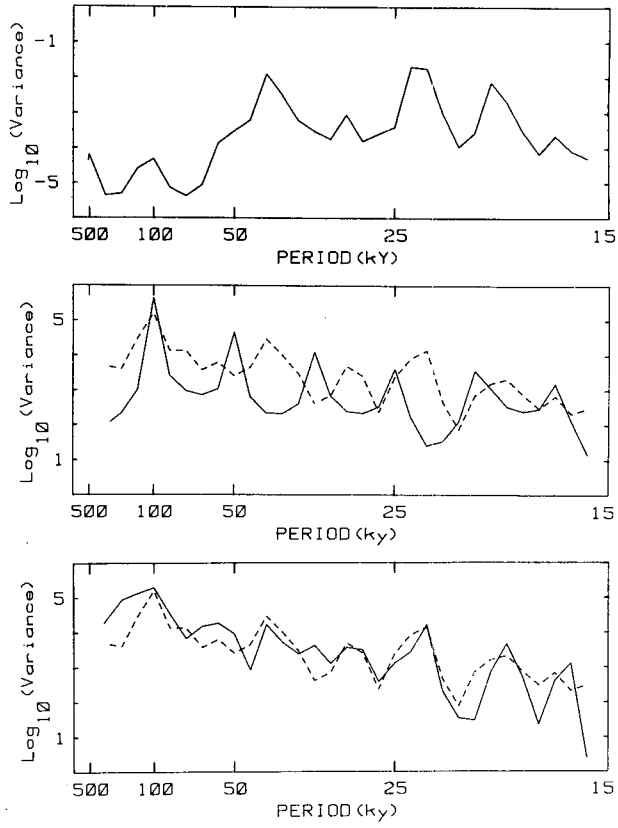


FIG. 6. Top: Variance spectrum of the composite forcing function $F_\chi$ based on a 1 Myr record. Middle: Variance spectrum of the *free* solution for $\zeta$ shown in Fig. 2 (solid curve), compared with the spectrum of the SPECMAP reconstruction of $\zeta$ shown in Fig. 4 (dashed curve), both for a 500 kyr record. Bottom: Variance spectrum of the *forced* solution for $\zeta$ shown in Fig. 4 (solid curve), again compared with the spectrum of the SPECMAP reconstruction (dashed curve), both for a 500 kyr record.

A similar level of agreement between the observed $\delta^{18}$O record and the output of an orbitally-forced nonlinear model has been obtained by Pollard (1982, 1983a,b), and to some extent also by Imbrie and Imbrie (1980), Oerlemans (1980, 1982), Birchfield *et al.* (1981), LeTreut and Ghil (1983) and Peltier and Hyde (1984). Bedrock response plays a dominant role in all of these models, except that of Imbrie and Imbrie (1980); and *free* oscillations of period near 100 kyr are absent in all these models except that of Oerlemans (1982) in which case, however, this free periodic variability seems to be quite sensitive to the choice of parameters. In the study by LeTreut and Ghil (1983) a model having a free periodic response of only 10 kyr can produce a large 100 kyr oscillation as a nonlinear resonant effect of forcing primarily at the precessional periods of 19 and 23 kyr. Thus it would appear that one distinguishing property of our present model is that *in the absence of any forcing* it would still yield a fairly robust near-100 kyr variability (Fig. 2) that could conceivably account for the obser-

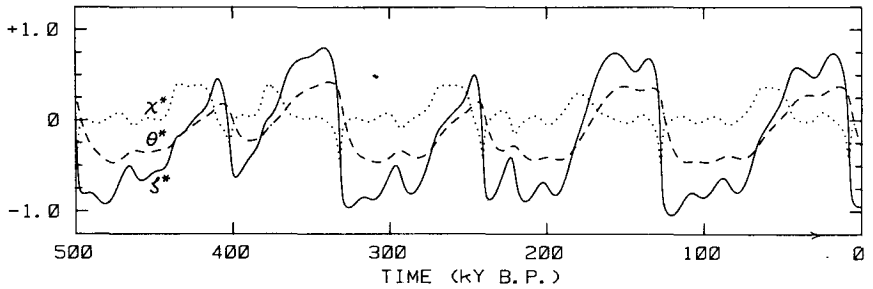


FIG. 7. Forced solution of the system (1), (2) and (3) showing the variation of $\chi$ (dotted) and $\theta$ (dashed), as well as $\zeta$ (solid, shown previously in Fig. 4). Nondimensional units are $\zeta^* = 1.45\ Z^{-1}\ \zeta'$, $\chi^* = 0.75\ X^{-1}\ \chi'$, and $\theta^* = 0.96\ \Theta^{-1}\ \theta'$, where $Z$, $X$ and $\Theta$ are arbitrary characteristic ranges of $\zeta'$, $\chi'$, and $\theta'$ during the Quaternary.

vations as a particular stochastic realization. It remains to be determined whether such a near-100 kyr free variability is necessary to account for the observed late Quaternary ice variations.

It would, of course, be desirable to verify the models predictive capability against independent data. Unfortunately, the future variation over thousands of years is unknowable. If we go backward in time to the early Quaternary the evidence points to the existence of a different mode of variability in which the 100 kyr period is much reduced (Start and Prell, 1984), indicative of a structural change (or bifurcation) involving a change in a parameter representing a key feedback. It will be of interest to try to identify and physically interpret this control parameter within the framework of our model.

As a potentially more viable test of the validity of our model, we show in Fig. 7 the simultaneous variations in the two other dependent variables predicted; i.e., marine/marginal ice mass $\chi$, and mean ocean temperature $\theta$. As noted in SS, there is as yet very little hard evidence concerning the long-term variations of these quantities. However, if we assume the amplitude of our ice mass solution $\zeta^*$ is roughly that of the SPECMAP (Imbrie *et al.*, 1984) estimate of continental ice mass $\hat{\zeta}^*$ (as pictured in Fig. 4), and also assume that $\theta$ bears some relation to the surface water temperatures in the low and middle latitudes where the SPECMAP cores were located, then the departures between the two curves in Fig. 4 should constitute an independent estimate $\hat{\theta}^*$ of the departures of ocean temperature from its equilibrium value. That is,

$$\hat{\theta}^* \approx k(\zeta^* - \hat{\zeta}^*),$$

where $k$ is an arbitrary constant of proportionality chosen to yield the same amplitude for $\hat{\theta}^*$ as for $\theta^*$. In Fig. 8 we plot $\hat{\theta}^* = 0.6(\hat{\zeta}^* - \zeta^*)$, along with our theoretical value of $\theta^*$ that was shown in Fig. 7 (dashed curve). The agreement is fairly good for the whole half-million year record, and in particular, there is good agreement with the detailed observational results of Dodge *et al.* (1983) for the "stage 5" interglacial variations between 125 and 80 kyr BP where independent sea-level estimates are available.

A further prediction that can be made from our model, unfortunately even less susceptable to geological verification, concerns the fluctuations in the net radiation at the top of the atmosphere $\tilde{N}^\uparrow$ (i.e., the difference between incoming solar radiation and outgoing longwave radiation averaged over the globe at the outer limit of the atmosphere) that must accompany the variations in $\zeta$, $\chi$ and $\theta$ shown in Fig. 7. As noted by Saltzman (1977, 1983)

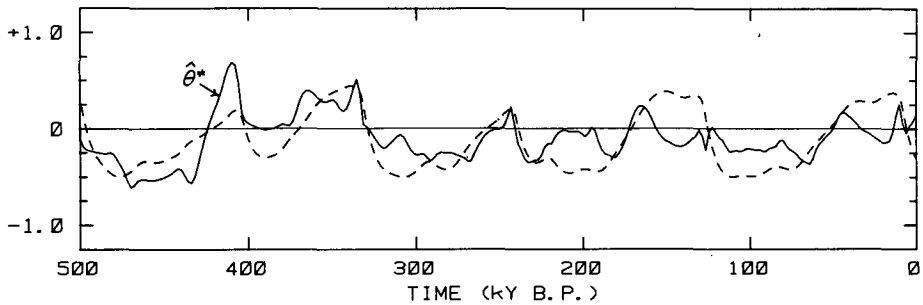


FIG. 8. Variation of $\hat{\theta}^* = 0.6(\zeta^* - \hat{\zeta}^*)$ (the departure of the theoretical continental ice mass curve $\zeta^*$ from the SPECMAP $\delta^{18}O$ curve $\hat{\zeta}^*$, shown in Fig. 4) versus the theoretical $\theta^*$ curve shown in Fig. 7.

$$\tilde{N}^{\downarrow} \approx -\frac{L_f}{\sigma}\frac{d(\zeta+\chi)'}{dt} + \frac{c_w M_w}{\sigma}\frac{d\theta'}{dt}, \qquad (8)$$

where $c_w$ is the specific heat of ocean water ($4 \times 10^3$ J kg$^{-1}$ K$^{-1}$ and $M_w$ is the mean mass of the world ocean ($1.4 \times 10^{21}$ kg). The variations of $N^{\downarrow}$ corresponding to our solution are shown in Fig. 9, assuming $Z = 5 \times 10^{19}$ kg, $X = 10^{18}$ kg, and $\theta = 3$ K. Thus, according to our model, periods of rapid deglaciation are marked by a spike of unusually large net incoming radiation.

## 5. Sensitivity and robustness

As discussed in Saltzman and Sutera (1984), the *free* solution shown in Fig. 2 is fairly robust, varying little for changes of ±10 percent in all the coefficients except $a_2$ and preserving its structural form for a relatively high level of additive white noise. We have already noted that our present forced solution for the last 500 kyr is also relatively insensitive to small changes in the forcing coefficients $\alpha$, $\beta$, and $\gamma$, as well as to the presence of noise, and to the initial conditions at 1 Myr BP. We now discuss in more detail the sensitivity of the *forced* solution shown in Fig. 4 or 7 to small variations in all the coefficients appearing in the dynamical system (1), (2) and (3). The results are based on an extensive series of experiments to determine the range of values within which stochastically stable solutions are obtained of the structural form shown in Fig. 4, including phase. All runs were tested for stochastic stability for additive noise of amplitude $|R_x| = 2 \times 10^{-5} X$ yr$^{-1}$ or larger.

With regard to the orbital coefficients $\alpha$, $\beta$ and $\gamma$, we find that when we hold all other coefficients constant the solution is unchanged when $0.70 \leqslant (\beta/\beta_0) \leqslant 1.45$ and $0.75 \leqslant (\gamma/\gamma_0) \leqslant 1.25$, for $\alpha = \alpha_0$; and is unchanged when $0.05 \leqslant (\alpha/\alpha_0) \leqslant 1.75$ for $(\beta, \gamma) = (\beta_0, \gamma_0)$, where $\alpha_0$, $\beta_0$, and $\gamma_0$ are the particular values used to obtain the solution shown (see Section 4). Outside of this parameter domain, solutions of similar structure can still be obtained but they begin to be unstable in the presence of white noise. It would appear that to obtain a stochastically stable solution agreeing with observations to the extent shown in Fig. 4 one must include not only the obliquity and precessional forcing of amplitudes $\beta$ and $\gamma$ within the limits given, but also at least some small forcing due to the pure eccentricity effect $\alpha > 0.05\alpha_0 = 0.35 \times 10^{-6} X$ yr$^{-1}$. In the case of this eccentricity forcing we have also shown that the solution is unaffected if the 100 kyr narrow-band forcing given by Imbrie *et al.* [1984, Fig. 3 (top)] is used instead of the broad-band eccentricity given here as $A(t)$ in Fig. 3 (top) which includes a marked 400 kyr periodicity as well as the 100 kyr periodicity. These "pacemaking" properties of small external forcing of a robust free nonlinear oscillation have been studied by Nicolis (1984) and are now being studied further in the context of the present model.

We also find that the solution shown in Fig. 4 is preserved if the coefficients $a$, $b$, and $c$ appearing in (1), (2), and (3), respectively, are varied within the percentage limits portrayed by the shaded area in Fig. 10, keeping all other coefficients constant. This figure clearly reveals the relatively high sensitivity of the solution to variations in $a_2$ that was already apparent in the free solution; in addition, high sensitivities (albeit of lesser degree) are revealed for $b_0$, $b_3$, $b_5$, $c_0$ and $c_2$. However, the new solutions which appear when these coefficient limits are exceeded are not altogether unreasonable compared to the SPECMAP estimate of glaciation assuming no ocean temperature effect. As it turns out, there are two relatively stable *departure modes,* labeled I and II in Fig. 10, to which the solution bifurcates depending on whether the coefficient in question is increased or decreased. The time variation of $\zeta$ for these two departure modes are shown in Fig. 11 (Mode I, top; Mode II, middle) along with the SPECMAP reconstruction (dashed curves). We can see that departure mode I still constitutes a highly acceptable replication of the last three glacial cycles; and mode II, while failing to replicate the important last cycle, provides even better agreement with the first two cycles (500–300 kyr BP) than our primary solution. In fact, for certain values of several sensitive coefficients in narrow transitional ranges leading to mode II (indicated by the heavy stippling in Fig. 10) we obtain quite good replication

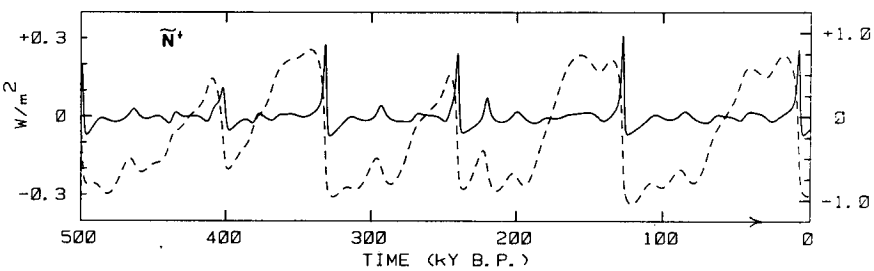


FIG. 9. Variations of net global incoming radiation accompanying the forced theoretical variations shown in Fig. 7, assuming $Z = 5 \times 10^{19}$ kg, $X = 10^{18}$ kg, and $\Theta = 3$ K (solid curve). Forced variations in $\zeta$, shown in Fig. 4, 5 and 7, are repeated for comparison (dashed curve).

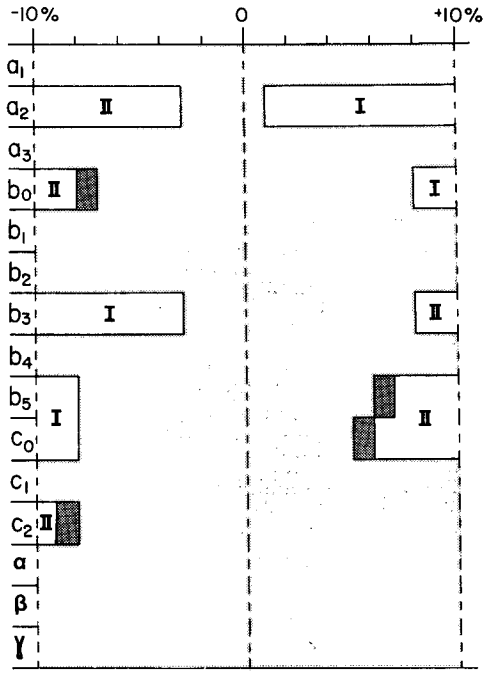


FIG. 10. Structure of the solution as a function of percentage change in individual coefficients in (1), (2) and (3), with all other coefficients fixed. Shaded values indicate no structural change from the solution shown in Fig. 4 or 7. Values denoted by I and II denote new modes having the structural forms for $\zeta$ shown in Fig. 11, top and middle, respectively. Values denoted by dark stippling in some regions of transitions to mode II have the structural form for $\zeta$ shown in Fig. 11, bottom (i.e., mode II-a).

of the whole SPECMAP ice chronology over the last half-million years (see Fig. 11, bottom, mode IIa). With further numerical experimentation, perhaps involving changed weightings of the orbital forcing components, it may be possible to demonstrate that this last mode IIa solution is more structurally stable than is indicated by our present set of calculations.

In any event, our present analysis suggests that, according to the conceptual postulates of our model (SS), the correct magnitude of the following physical processes (assumed to be represented by the most sensitive coefficients) are most important in accounting for the observed ice age variations:

1) The control of snow accumulation on ice sheets exercised by peripheral marine ice formation and marginal extent of continental ice, assumed to be measured by $a_2$.

2) The control of marine ice shelf mass and extent exercised by ice sheets and ice stream flow, assumed to be measured by $b_0$.

3) The negative feedback on marine and continental marginal ice due to surface heat balance changes as a function of latitudinal extent, assumed to be measured by $b_3$.

4) Control of marine ice extent by ocean temperature, assumed to be measured by $b_5$.

5) Control of bulk ocean temperature exercised by (i) sea level change and (ii) ice sheet variations over the source regions where deep water and thermohaline circulation are produced, assumed to be measured by $c_0$, and

6) The eddy thermal diffusion rate for the ocean, assumed to be measured by $c_2$. (Our primary solution is exhibited for a range of values of the "time constant" $c_2^{-1}$ between 6100 and 7500 yr.)

## 6. Discussion and conclusions

In essence, the model of the late Quaternary ice age variations proposed here represents an attempt to provide a quantitative dynamical structure to some of the more qualitative physical ideas proposed by Denton and Hughes (1981, 1983). As distinct from other models, in our scenario the main players are the terrestrial ice component $\zeta$, the essentially "marine" ice component $\chi$, and a non-cryospheric "climate" component that we identify with the mean ocean temperature $\theta$. As noted in SS, such processes as shelf ice buttressing, downdraw, sea-level change, are all assumed to be represented in our internal feedbacks.

While we do not underestimate the possible role of bedrock response, and in fact would deem it desirable to include it as a fourth prognostic variable in a future model, we are exploring here the limits to which one can go in accounting for the ice age variations in its absence as an explicit variable. We believe that we have demonstrated that one can go at least as far as the bedrock models in this regard. We have also provided further theoretical evidence that earth-orbital radiation variations can play the critical role as a "pacemaker" for the ice age variation as was proposed by Hays *et al.* (1976).

Many fundamental questions remain to be addressed in more detail. For example,

1) How does small amplitude periodic forcing control phase in a complex nonlinear oscillatory system and is there a good physical interpretation for this "phase locking" phenomenon?

2) How do we measure the sensitivity of the structural form (e.g., period, and asymmetry) of a solution to the values of the system parameters?

3) What crucial parameters have changed to permit the oscillatory behavior in the late Quaternary that was absent in the early Quaternary, and what are their physical interpretations?

4) How can we deepen our understanding of the physical processes associated with the sensitivities revealed for certain parameters of the model (e.g., $a_2$)?

5) Can we deduce the geographic spatial distribution of ice mass that must be associated with the *global* values we treat here (e.g., Saltzman 1984)?

6) Can we apply newly developing mathematical

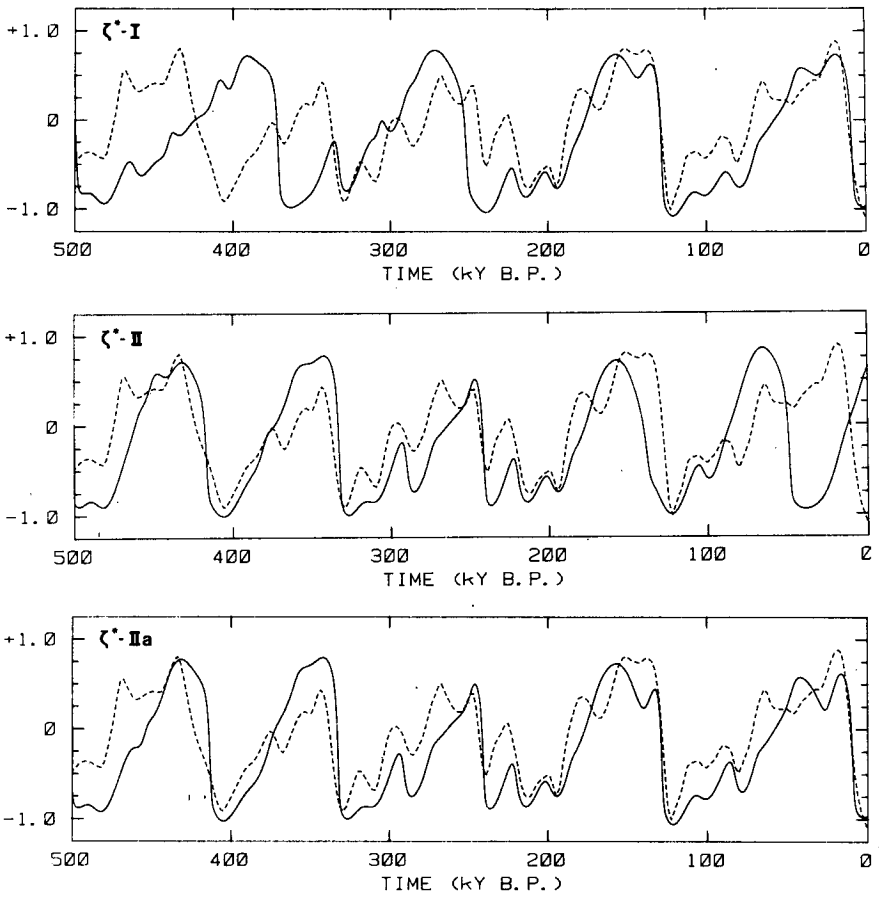


FIG. 11. Modes of $\zeta$ variation to which the solution bifurcates for changes in coefficients shown in Fig. 9. Mode I (top), mode II (middle) and mode IIa (bottom).

methods (e.g., Packard, *et al.*, 1980) to systematize the inductive process of constructing ever-improving dynamical systems models of long term climatic change?

The answers to these and other relevant questions are currently being pursued.

*Acknowledgments.* This work is based upon research supported by the Division of Atmospheric Sciences, National Science Foundation, under Grants ATM-7925013 and ATM-8411195 at Yale University. We are grateful to Alfonso Sutera for longstanding helpful discussions of the problem area treated, and to John Imbrie for making available the SPECMAP ice chronology and the earth-orbital forcing functions.

## REFERENCES

Berger, A. L., 1977: Long-term variation of the earth's orbital elements. *Celestial Mech.*, **15**, 53–74.

Birchfield, G. E., J. Weertman and A. T. Lunde, 1981: A paleoclimate model of northern hemisphere ice sheets. *Quat. Res.*, **15**, 126–142.

Broecker, W. S., 1984: Terminations. *Milankovitch and Climate*, A. Berger, J. Imbrie, J. Hays, G. Kukla, and B. Saltzman, Eds., Reidel, 87–698.

Denton, G. H., and T. J. Hughes, 1981: The Arctic ice sheet: An outrageous hypothesis. *The Last Great Ice Sheets*, G. H. Denton and T. J. Hughes, Eds., J. Wiley and Sons, 437–467.

——, and ——, 1983: Milankovitch theory of ice ages: Hypothesis of ice-sheet linkage between regional insolation and global climate. *Quat. Res.*, **20**, 125–144.

Dodge, R. E., R. G. Fairbanks, L. K. Benninger and F. Maurrasse, 1983: Pleistocene sea levels from raised coral reefs of Haiti. *Science*, **219**, 1423–1425.

Hays, J. D., J. Imbrie and N. J. Shackleton, 1976: Variations in the earth's orbit: Pacemaker of the ice ages. *Science*, **194**, 1121–1132.

Imbrie, J., and J. Z. Imbrie, 1980: Modeling the climatic response to orbital variations. *Science*, **207**, 943–953.

——, J. D. Hays, D. G. Martinson, A. McIntyre, A. C. Mix, J. J. Morley, N. G. Pisias, W. L. Prell and N. J. Shackleton, 1984: The orbital theory of pleistocene climate: Support from a revised chronology of the marine $\delta^{18}O$ record. *Milankovitch and Climate*, A. Berger, J. Imbrie, J. Hays, G. Kukla, and B. Saltzman, Eds., Reidel, 269–305.

Kutzbach, J. E., 1981: Monsoon climate of the early holocene: Climate experiment with the earth's orbital parameters for 9000 years ago. *Science*, **214**, 59–61.

LeTreut, H., and M. Ghil, 1983: Orbital forcing, climatic interactions, and glaciation cycles. *J. Geophys. Res.*, **88**, 5167–5190.

Milankovitch, M., 1920: *Theorie Mathematique des Phenomenes Thermiques Produits par la Radiation Solaire*. Gauthier-Villers, 339 pp.

Nicolis, C., 1984: Self-oscillations and predictability in climate dynamics—Periodic forcing and phase locking. *Tellus,* **A36,** 217–227.

Oerlemans, J., 1980: Model experiments on the 100,000-yr glacial cycle. *Nature,* **287,** 430–432.

——, 1982: Glacial cycles and ice-sheet modelling. *Clim. Change,* **4,** 353–374.

Packard, N. H., J. P. Crutchfield, J. D. Farmer and R. S. Shaw, 1980: Geometry from a time series. *Phys. Rev. Lett.,* **45,** 712–716.

Peltier, W. R., and W. Hyde, 1984: A model of the ice age cycle. *Milankovitch and Climate,* A. Berger, J. Imbrie, J. Hays, G. Kukla, and B. Saltzman, Eds., Reidel, 565–580.

Pollard, D., 1982: A simple ice sheet model yields realistic 100 kyr glacial cycles. *Nature,* **296,** 334–338.

——, 1983a: A coupled climate-ice sheet model applied to the Quaternary ice ages. *J. Geophys. Res.,* **88,** 7705–7718.

——, 1983b: Ice-age simulations with a calving ice-sheet model. *Quat. Res.,* **20,** 30–48.

Saltzman, B., 1977: Global mass and energy requirements for glacial oscillations and their implications for mean ocean temperature oscillations. *Tellus,* **29,** 205–212.

——, 1983: Climatic systems analysis. *Advances in Geophysics,* Vol. 25, Academic Press, 173–233.

——, 1984: On the role of equilibrium atmospheric climate models in the theory of long-period glacial variations. *J. Atmos. Sci.,* **41,** 2263–2266.

——, and R. E. Moritz, 1980: A time-dependent climatic feedback system involving sea-ice extent, ocean temperature and $CO_2$. *Tellus,* **32,** 93–118.

——, and A. Sutera, 1984: A model of the internal feedback system involved in late Quaternary Climatic variations. *J. Atmos. Sci.,* **41,** 736–745.

——, —— and A. R. Hansen, 1984: Earth-orbital eccentricity variations and climatic change. *Milankovitch and Climate,* A. Berger, J. Imbrie, J. Hays, G. Kukla, and B. Saltzman, Eds., Reidel, 615–636 pp.

Start, G. G., and W. L. Prell, 1984: Evidence for two Pleistocene climatic modes: Data from DSDP site 502. *New Perspectives in Climate Modelling,* A. L. Berger and C. Nicolis, Eds., Elsevier, 3–22.

Vernekar, A. D., 1972: Long-period global variations of incoming solar radiation. *Meteor. Monogr.,* No. 34, Amer. Meteor. Soc., 21 pp. + tables.